Union College
Union | Digital Works

Honors Theses | Student Work

6-2005

Inclusion of customized quantum dots into laponite based nanocomposites

Jennifer Rae Eliseo
Union College - Schenectady, NY

Follow this and additional works at: https://digitalworks.union.edu/theses

 Part of the Chemistry Commons

Recommended Citation
Eliseo, Jennifer Rae, "Inclusion of customized quantum dots into laponite based nanocomposites" (2005). *Honors Theses*. 2092.
https://digitalworks.union.edu/theses/2092

This Open Access is brought to you for free and open access by the Student Work at Union | Digital Works. It has been accepted for inclusion in Honors Theses by an authorized administrator of Union | Digital Works. For more information, please contact digitalworks@union.edu.

UN
82
E43i
2005

INCLUSION OF CUSTOMIZED QUANTUM DOTS INTO LAPONITE BASED NANOCOMPOSITES

By

Jennifer Rae Eliseo

****

Submitted in partial fulfillment

of the requirements for

Honors in the Department of Chemistry

UNION COLLEGE

June 2005

ABSTRACT

ELISEO, JENNIFER Inclusion of customized quantum dots into Laponite based nanocomposites. Union College Department of Chemistry, June 2005.

Quantum dot (QD) semiconductor nanocrystals offer unique electronic, magnetic, and optical properties that can be used in advanced materials applications including optoelectronics, catalysis, sensing, and quantum computing. Tailoring of quantum dot surface coatings allows for control of self-assembly and facile inclusion into various host matrices. Querner and colleuges have provided a novel synthetic route to graft aniline tetramer units onto quantum dots via a disulfide bridge. A key goal of our work has been the optimization of this synthesis for inclusion of functionalized QDs within Laponite/polyaniline nanoscaffolds. Uv/visible and fluorescence spectroscopy were used to study frequency resonance energy transfer within our QD/linker/tetramer/Laponite system. Our studies illustrate that Laponite affords an ideal host framework for realization of QD based light emitting diodes and photovoltaics.

ACKNOWLEDGEMENTS

I thank my family for all of their loving support as I have pursued my dreams and ambitions. They have been with me through the good times and the bad times. They have been my inspiration through some of life's most challenging circumstances.

I also thank my advisor, Professor Michael Hagerman, for allowing me to design my thesis project and carry out new, cutting-edge research. In addition, I thank Professor Brian Cohen and Professor Joanne Kehlbeck for their unique and much needed contributions to this research. I would like to thank my colleagues that have worked on this project: Mayrita Arrandale, Evan Leibner, Nate Davis, Amy Payeur, Melissa Fox, and Michael Nolan. Also, the Union College Chemistry Department for the highest-quality teaching I've ever known and for challenging me to go further academically and personally than I ever imagined.

Table of Contents

Table of Figures and Tables

1. Introduction

Many of the strategies proposed in nanoscience to bridge the divide between top-down and bottom–up methods of nanomaterials synthesis hinge on an understanding of how to attach molecules to each other to realize macroscopic structures. Self-assembled nanostructures use these supramolecular chemistry approaches to take advantage of encoded information within the components of the nanostructure building block. Self-assembly has been described as the autonomous organization of components into patterns or structures without human intervention.[1] Self-assembly offers unique routes for bottom-up fabrication of nanocomposites. The phenomenon of self-assembly has recently gained attention as novel routes to fabricate organic-inorganic nanocomposites.

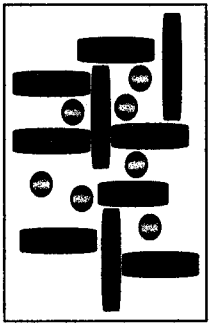

Figure 1. Organic-Inorganic Nanocomposite. (Discs represent host and spheres represent guest).

Organic-inorganic nanocomposites are systems that are composed of an organic guest that is embedded in an inorganic host (Figure 1). These hybrid nanostructures can exhibit properties superior to those of their individual components. Therefore, these systems have become the focus of many research groups across the fields of chemistry, physics, engineering, natural sciences, and biology.[2,3,4,5] Our study focuses on the inclusion of quantum dot guests into Laponite clay host assemblies. These nanocomposites hold promise for the future development of chemical sensors,[6] light-emitting diodes,[7] and photovoltaics.[8]

The "guests" in our system are nanoscale semiconductor particles[9] (quantum dots, or QDs) (Figure 2). QDs have a wide variety of applications due to their unique material

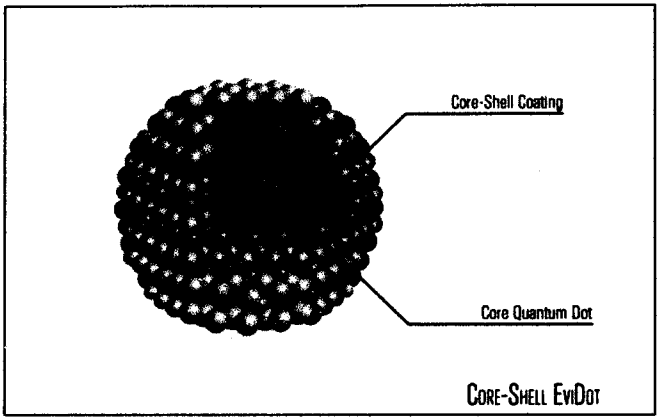

Figure 2. Structure of quantum dot guest. Adapted from www.evidenttech.com.

features that include tunable absorption and emission patterns, stability against photobleaching, flexible molecular coupling, and quantum yields higher than traditional organic dyes.[10] Semiconductor nanocrystals are unique in that their diameter is only 2-10 nm across and the addition or subtraction of just a few atoms can alter the emission wavelength of the nanocrystal. An increase in nanocrystal size will result in increased emission wavelength (Table 1). Our interests in quantum dot materials lie in the integration of functionalized nanoparticles into a chemical sensor system.

Trade Name	Emission Peak	Crystal Diameter (nm)
Lake Placid Blue	490 +/- 10	2.0
Adirondack Green	520 +/- 10	2.4
Catskill Green	540 +/- 10	2.8
Hops Yellow	560 +/- 10	3.2
Birch Yellow	580 +/- 10	3.5
Fort Orange	600 +/- 10	4.1
Maple-Red Orange	620 +/- 10	5.0

Table 1. Comparison of nanocrystal diameter (nm) and emission wavelength (nm).

It is important to consider the surface of nanocrystal quantum dots and the associated chemistry that can accompany the functionalization of a quantum dot surface. Conventional quantum dots include an outer trioctylphosphine oxide (TOPO) layer that contributes to the nanocrystal's hydrophobic nature and allows it to be soluble in common organic solvents. However, TOPO does not completely cover the dot's outside shell, which create traps that cause quenching and reduced emission.[11]

Development of new nanocrystal surface ligands[12,13,14] has begun to open the door to various applications for semiconductor nanocrystals. Many new functions include nanoelectronics,[15] biolabels and biosensors,[13,16] photovoltaic and solar cells,[8] light-emitting diodes,[7,13] and various new nanocrystal/organic/inorganic hybrid materials.[8] Querner and coworkers[8] have developed nanocrystal surface ligands containing a carbodithioate (-C(S)S$^-$) functional group, which serves as an anchor to the quantum dot shell surface. The ligand is then grafted with aniline tetramer molecules. These aniline tethers can be useful for applications in light-emitting diodes and photovoltaic cells because charge transfer can occur through the conjugated pi system.[17] While literature shows that traditional nanocrystals have been entrapped in various matrices, including

sol-gel derived silica spheres,[18] our nanohybrid assembly within Laponite clay is a novel approach with various applications in sensing and electronics.

Laponite is an ideal inorganic host matrix due to the lamellar (2-D) nanospace layering of the smectite.[19] Additionally, the excellent optical transparency of Laponite enhances its versatility as a chemical sensor based on photophysical properties. Laponite offers unique sensing capabilities as films can be coated on various substrates through facile self-assembly from the aqueous phase. The architecture of the smectite-type clays consist of a 2:1 ratio of tetrahedral to octahedral oxide layers and an intergallery region between each tetrahedral-octahedral-tetrahedral (TOT) layer (Figure 3). The intergallery regions have the ability to conform to the shape and size of the guest molecule and the ability to cation exchange. This allows inclusion of the guest into the Laponite host's lamellar ordered tactoid matrix in films.[20]

The Laponite utilized in our studies was donated by Southern Clay Products as sodium Laponite. Past studies have shown that zinc-exchanged Laponite reduces phase separation in films. Therefore, we exchanged the sodium for zinc through facile preparation methods in order to enhance film quality.

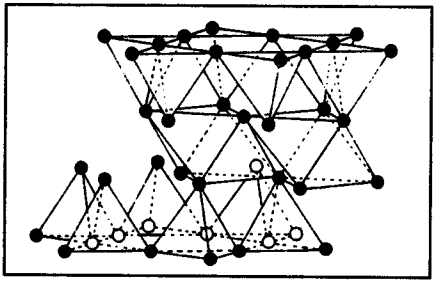

Figure 3. Tetrahedral-Octahedral-Tetrahedral (TOT) layering of Laponite clay host.

1.1 Chemical Sensor Design

Needs for new and more efficient chemical sensors are apparent due to the stricter EPA regulations and the growing complexity of systems in which chemical sensing is required. Sensors are needed to detect numerous chemicals including: CO, SO_2, NO_x, O_3, H_2, and various hydrocarbons. Currently the EPA has regulations for performing a standardized test of groundwater and soil samples using modern analytical laboratory equipment. A significant cost savings at both the state and federal levels would occur if chemical sensors integrated with pattern recognition techniques were developed for continuous on-site environmental monitoring, specifically for analyzing groundwater well and soil samples. Other possible uses for chemical sensors include fuel cells, automobiles, jet turbines, and safety sensors.[6] Interest in our nanohybrid quantum dot based system lies in the integration of functionalized nanoparticles into a chemical sensor system with enhanced selectivity and sensitivity for detection of BTEX hydrocarbons (benzene, toluene, ethyl benzene, and xylenes) in various environments.

In addition to our QD/Laponite system, we aim to develop a smart, robust, and versatile nanosensor system that includes Rhodamine dyes along with functionalized quantum dots and Laponite (Figure 4). This system offers various advantages including the bottom-up self-assembly of multiarray sensor films, capacity to use a single UV excitation source, and an easy-to-use sensor system.

Rhodamine requires a specific wavelength to be excited; usually this necessitates laser light. However, it is possible to use a cheap UV light source to excite quantum dots. The nanocrystals emission could then be used to "pump" (via Fluorescence Resonance Energy Transfer (FRET)) various Rhodamine dyes at a specifically tuned wavelength so

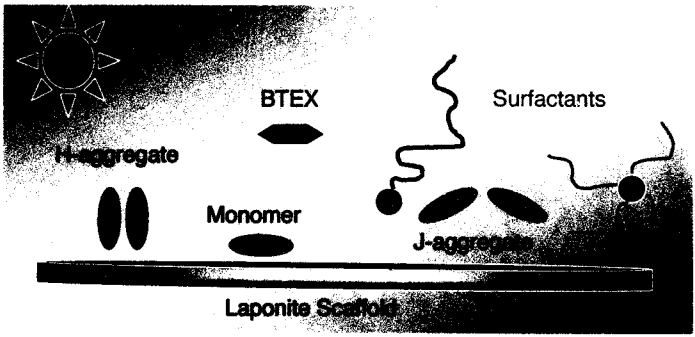

Figure 4. Depiction of overall hydrocarbon sensor system including QD/Laponite nanocomposite with various surfactants to control analyte exposure to clay surface and Rhodamine aggregates (H (non-fluorescent, pi stacked aggregates), J (fluorescent, head-to-tail aggregates), and monomer (fluorescent monomers)).

that Rhodamine/Laponite sensor systems may have higher sensitivity for the detection of BTEX molecules in ambient, soil, and ground water systems. Upon introduction of the analyte, if the hydrocarbon compounds complexes with the J-aggregated dimer, chromophore luminescence maxima, emission intensity, and lifetime will be affected.

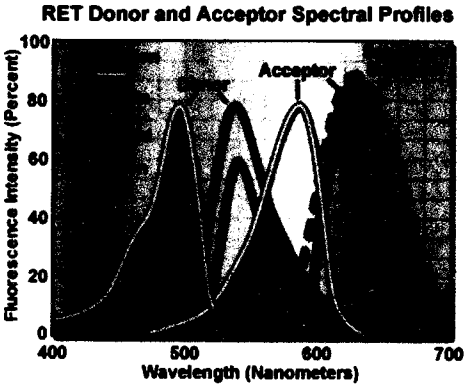

Figure 5. Model of Fluorescence Resonance Energy Transfer. Adapted from http://microbackup.magnet.fsu.edu/primer techniques/fluorescence/fluorescenceintro.html

Coupled donor and acceptor molecules can undergo FRET[21,22,23] when the emission of the donor molecule overlaps with the acceptors excitation (Figure 5). The molecules must close enough to each other to allow energy transfer (i.e. Our useful Laponite matrix holds everything together in nanopore space). When energy is transferred non-radiatively from the donor to the acceptor there is quenching of donor emission and increased intensity in acceptor emission.

In summary, this proposed nanocomposite sensor system has many advantages. The transparent Laponite host will not allow for any unnecessary loss of emission. In addition, the system can be fabricated through facile aqueous exchange methods. Also, it utilized a cheap UV light source and is easy to use in the field for the detection of hydrocarbons by simply observing changes in the intensity or shape of the emission peak of the nanocomposite.

1.2 Light-emitting diodes

While the objective of this research project has been to develop novel chemical sensor systems based on the inclusion of Rhodamine dyes with functionalized quantum dots into Laponite clay, there are alternative applications

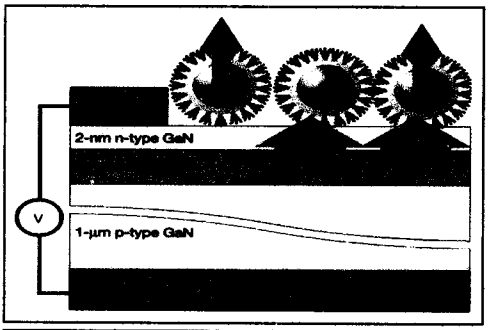

Figure 6. Design scheme and operation of QLED. Adapted from Archermann, M.; Petruska, M.A.; Kos, S.; Smith, D.L.; Koleske, D.D.; and Klimov, V. *Nature*, 2004, *429*, 10.

for customized nanocrystals that should be explored, mainly quantum dot based light-emitting diodes (QLEDs).[7,24]

Archermann and coworkers at Los Alamos National Laboratory have recently developed QLEDs. These devices are thin-film LEDs that contain an active layer of II-VI semiconductor nanocrystal between metal electrodes. Photons emitted for the traditional LED encounter the discrete energy bands specific to the nanocrystal. Because the bandgap of a quantum dot can be altered with the addition or subtraction of just a few atoms, QLEDs can be customized to a predetermined fixed emission wavelength ranging the whole visible spectrum.

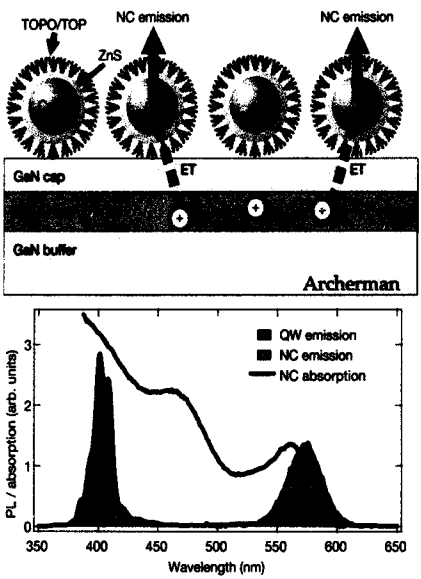

Figure 7. FRET occurring in QLED. Adapted from Archermann, M.; Petruska, M.A.; Koe, S.; Smith, D.L.; Koleske, D.D.; and Klimov, V. *Nature*, 2004, *429*, 10.

Archermann's design (Figure 6) includes a monolayer of TOPO-covered CdSe quantum dots on top of a quantum well of InGaN. This quantum well is a thin sheet of semiconductor sandwiched between two barrier layers. Electron-hole pairs recombine in the quantum well and produce resonant energy transfer (FRET) through

dipole-dipole interactions. In turn, the nanocrystals are excited by the energy transfer and emit a specific wavelength determined by the crystal size (Figure 7).

Archermann's design proposed that the monolayer of quantum dots are embedded within a polymer matrix. It may be possible to replace the QD/polymer composite with one of quantum dots and Laponite.

There are many reasons why these novel QLEDs are preferred over traditional light-emitting diodes. First, quantum dots can be grown by simple, inexpensive synthetic methods. As mentioned before, there is also the advantage of tunable light emission by alteration of the nanocrystal's bandgap. In addition, quantum dots can be designed to emit any visible and infrared wavelengths. Also, the high quantum yields of semiconductor nanocrystals eliminate all light scattering and the associated optical losses observed in traditional LEDs. Finally, QLEDs are able to run at low voltages (between 1-4 volts) making operation costs low as well.

1.3 Photovoltaics

In addition to light-emitting diodes, another useful application for quantum dots include photovoltaics and solar cells. The idea of a solar cell is to convert solar light energy into electrical current.[25]

Functionalized quantum dots can be utilized in these systems by embedding the nanocrystals into solar panel material. The solar panel absorbs photons of light from the sun. The functionalized quantum dots in which the functional group contains a conjugated pi system would then be able to, hypothetically, convert the light energy to electrical current. The quantum dot core would absorb the photon and electron charge transfer could occur out through the pi system, creating electrical current (Figure 8).

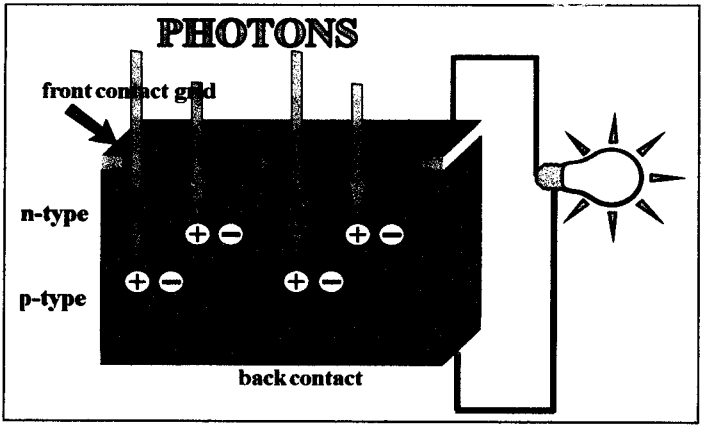

Figure 8. Schematic of a solar cell in which functionalized quantum dot could be utilized. Adapted from http://www.specmat.com/Solar%20Cell%20Description.jpg

Querner and coworkers[8] have shown that the energy levels of a quantum dot can be overlapped with those of an aniline tetramer tether. Their customized quantum dots may be useful in solar cell applications because, while emission of the quantum dot is completely quenched by the added ligands, the quantum dot still absorbs at the first exciton peak. This could mean that a photon of light that is absorbed by the quantum dot

could be cause electron charge transfer to occur through the pi system of the aniline tetramer in the form of electrical energy. Skaff and coworkers have studied this in their work on nanocrystals embedded in PPV polymers. The increased contact between the nanocrystal and the polymer was found to facilitate energy transfer.[13]

1.4 Goals

The goal of this project is explore uses for quantum dots in chemical sensors, light-emitting diodes, and photovoltaics. We aimed to first find an ideal concentration of quantum dot within Laponite that would provide the best emission. Then, we explored ways in which the nanocrystal surface could be tailored to better fit into the proposed Rhodamine/Surfactant/QD/Lap nanocomposite system. Optical studies were conducted of TOPO-covered quantum dots within the Laponite clay and of the tailored quantum dots (as done by Querner and coworkers) to be used in the Laponite system. Our studies illustrate that Laponite affords an ideal host framework for realization of QD based chemical sensors, light emitting diodes, and photovoltaic cells.

2. Optimal Quantum Dot Concentration

2.1 Preliminary Studies

In our initial studies we investigated systems with Rhodamine 6G/Hops Yellow QD (in hexane)/Laponite and Rhodamine 110/TMCA/Lake Placid Blue (Water soluble)/Laponite nanocomposites. These studies were used to study ideal concentrations of nanocrystal that might be needed to pump the Rhodamine.

The first system (Rhodamine 6G/Hops Yellow QD (in hexanes)/Laponite) was studied in three ways. One set of films were made with only Rhodamine 6G and Laponite, another set was made with 0.5% CEC Rh6G in Laponite (this is the cation

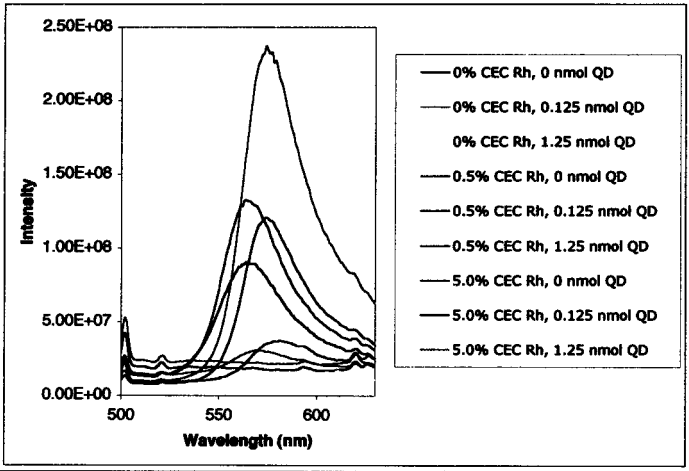

Figure 9. Photoluminescence emission of Rh6G/HYQD(in hexanes)/Lap composite at various loadings. Excitation wavelength 352nm.

exchange capacity that provides the most ideal emission of Rhodamine 6G), and a third set with a high loading of Rh6G in Laponite (5.0% CEC). Each set of films had loadings

of quantum dot as follows: 0 μL, 1 μL (0.125 nmol), and 10 μL (1.25 nmol) (Hops Yellow: MW of core = 20 μg/nmol.; Concentration: 2.5mg/mL). (Note: all samples are a total of 1.25 mL). In addition, all samples included 600 μL of deionized water. The films made were studied with uv/visible and fluorescence spectroscopy.

The absorption of the Rh6G/HYQD/Lap system is dictated by the absorption of the Rhodamine. There is the usual H-aggregate shoulder along with the red shifted peaks at lower loadings of Rhodamine. It is important to note the peak around 360 nm that shows at higher loadings of Rhodamine. This may be due to another type of aggregation between the Rhodamine molecules.

The ideal excitation wavelength for any quantum dot is any wavelength under 400 nm. The J-aggregate (the most fluorescent aggregate) of Rhodamine 6G is excited at 550

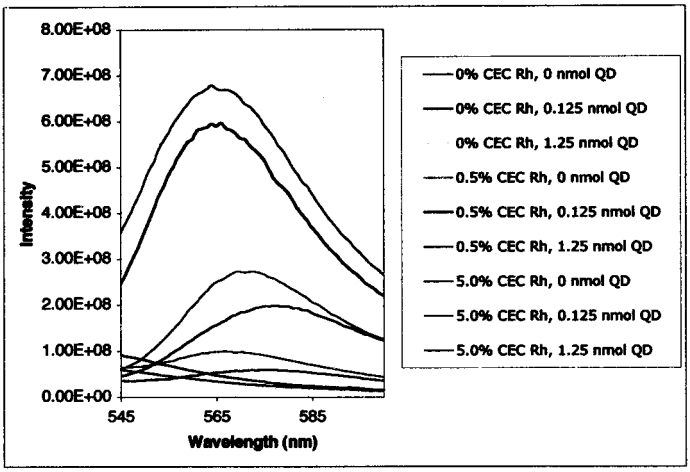

Figure 10. Emission of Rh6G/HYQD(in hexanes)/Lap composite. Excitation wavelength 530 nm.

nm. Figures 9 and 10 are emission spectra of the same system with different excitation wavelengths (352 nm vs. 530 nm). At the lower excitation wavelength, the samples that contain both Rhodamine 6G and quantum dot give intense emission peaks. However, if the quantum dots were being excited within the system, we would expect to see emission from the samples that contain quantum dot and no Rhodamine. At the higher excitation wavelength, the emission spectrum is indicative of the J-aggregate of Rhodamine 6G where quenching and red shifting occurs at higher Rhodamine loadings.

It is important to note that other studies with this system were explored using the same quantum dots in aqueous solutions and similar results were obtained. In addition, in future studies it would be advantageous to excite the samples at a wavelength where the Rhodamine does not absorb. That was attempted by using the excitation wavelength of 352 nm, however the absorbance spectra show that with increased concentration of the Rhodamine, a peak around 360 nm is apparent. Therefore, we may have been directly exciting the Rhodamine by using 352 nm light.

The second system studied was one that included the surfactant trimethylcetyl (TMCA). The films for the composite Rhodamine 110/TMCA/Lake Placid Blue (Water soluble)/Laponite were made in the same way and characterized with the same instruments and parameters (Lake Placid Blue: MW of core = 2.7μg/nmol; Concentration= 0.25mg/mL).

The absorption spectra of this system are different from the Rh6G system in that the peak around 360 nm is not present. This is probably due to the presence of surfactants that have been shown to turn aggregation on and off within

Rhodamine/Laponite systems.[26] In addition, the emission spectra (Figure 11) have reduced noise and a more obvious separation of the Rhodamine loadings based on intensity. It is suspected that the presence of TMCA (or other possible surfactants) provides better, more useful films for our studies because it reduces phase separation of the samples.

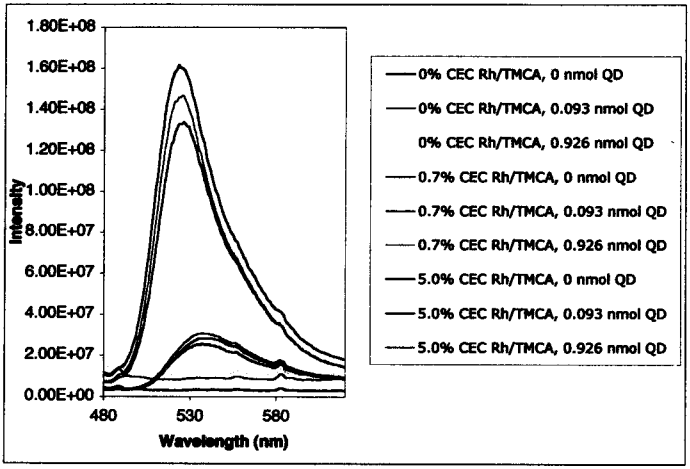

Figure 11. Emission of Rh110/TMCA/LPBQD/Lap composite. Excitation wavelength 333 nm.

Overall, theses preliminary studies have shown that because FRET cannot be proven directly, it is more advantageous to explore the components of the chemical sensor system individually and understand how they work, and then combine them to see how they function together. First, we explored an ideal concentration of quantum dot in Laponite that would have enough nanocrystal to give an intense, narrow emission from the quantum dot, but not so high that self-aggregation would occur.

2.2 Experimental

2.2.1 Preparation of Zinc Laponite Clay. 6.001 g of Na-Laponite clay ($Na_{0.7}[Li_{0.3}Mg_{5.5}Si_8O_{22}(OH)_4]$) (Southern Clay Products) was dissolved in 900 mL deionized water. The mixture was stirred for 30 minutes. Then 9 mL of $Zn(NO_3)_2$ was added and the solution was allowed to monodisperse overnight. Portions of the Laponite solution were centrifuged for 10 minutes at 10,000 rpm three times washing with 20 mL deionized water between runs. After final run, samples were redissolved in 30 mL deionized water and recombined all samples allowing to stir overnight. Product gave Zn-exchanged Laponite in solution of 3.82 mg/mL.

2.2.2 Preparation of quantum dots within Laponite clay. Adirondack Green quantum dots in water (MW of core = 9μg/nmol; Concentration= 0.25 mg/mL) were acquired from Evident Technology. Each film had a total of 1.25 mL of sample each including: 600 µL Zn-Laponite solution, increasing loadings of quantum dot (0, 50 (1.39 nmol), 100 (2.78 nmol), 200 (5.56 nmol), 300 µL (8.33 nmol)), and the remaining sample was deionized water. Samples were combined in Eppendorf microfuge tubes, shaken by hand, and then cast onto microscope slides and allowed to dry.

2.3 Results and Discussion

The inclusion of quantum dots within Laponite clay is an example of new self-assembled nanostructures. Figure 12 shows the absorbance of these films with increased loadings of quantum dot. As the quantum dot loading increases, the absorption of the film increases and becomes broader as observed at the first exciton peak at around 510nm.

Fluorescence spectroscopy of these films (Figure 13) shows that only at higher loadings emission can be observed, while at lower loadings it is not. This may be because there are not enough dots within the composite system to observe emission signal. For the highest loading (8.33 nmol), the intensity and narrow bandwidth (Full width at half-max ~25nm) are maintained. This may be a good concentration at which to do future studies of these systems.

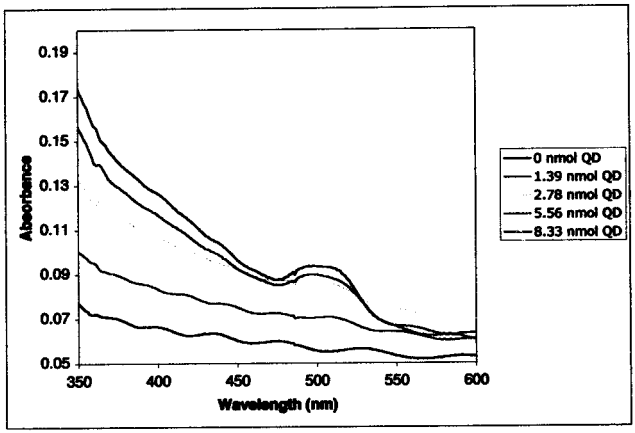

Figure 12. Absorption spectra of quantum dots in Laponite at increasing concentrations.

Semiconductor nanocrystals were successfully embedded into a Laponite clay host matrix and retained their broad absorption and narrow emission as observed in solution. This proves that the QD/Lap system may be useful in our chemical sensor design or quantum dot-based light-emitting diodes.

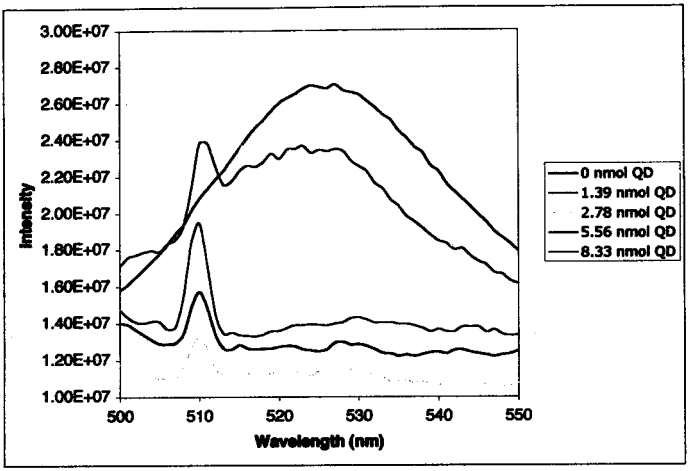

Figure 13. Emission Spectra of QD/Lap films with increasing QD loadings. Excitation wavelength 360 nm.

Archermann's QLED systems (Section 1.2) require the monolayer of quantum dots to be embedded into a polymer matrix (Figure 14). Our studies have shown a facile approach for embedding quantum dot nanocrystals into Laponite clay. This QD/Laponite system may be superior to QD/polymer system because the Laponite is a transparent host in which the quantum dots can be monodispersed without aggregation. Because of the transparency of Laponite, it may serve as a better host matrix for a light-emitting diode because more of the emitted light can be released, resulting in a more efficient system. Laponite also provides a better interface with silicon systems and increased thermal stability.

While Archermann has utilized TOPO covered quantum dots in these QLED systems, it is possible that nanocrystals that have been functionalized may offer a better system if they provide a more efficient route for energy transfer to the quantum dot without quenching the nanocrystal's emission signal.

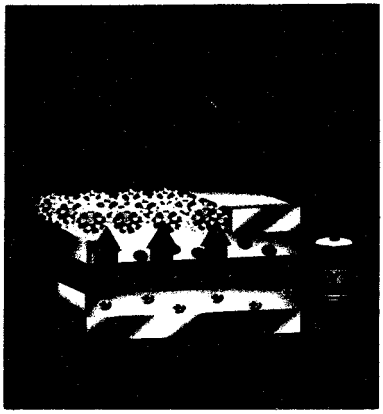

Figure 14. Energy transfer occurring in QLED. Adapted from http://sciencenow.sciencemag.org/cgi/content/full/2004/610/1.

In summary, quantum dots have been shown to enhance the properties of light-emitting diodes. We have synthesized the first QD/Laponite nanocomposite with potential applications as a quantum dot light-emitting diode. It is possible that our QD/Laponite system may serve as an ideal alternative current to polymer systems. In addition, customized quantum dots may allow for enhanced nanocrystal emission resulting more efficient light-emitting diode systems.

3. Functionalization of Quantum Dot Surfaces

Querner and coworkers provide a novel route for the synthesis of a quantum dot linker that can be utilized in the grafting of aniline onto a quantum dot surface (Figures 15 and 16). Further studies of this system and the control over the surface chemistry of quantum dot nanocrystals may provide useful information about its use in chemical sensors, light-emitting diodes, or photovoltaics by coupling into the energy levels of the semiconductors.

3.1 Experimental

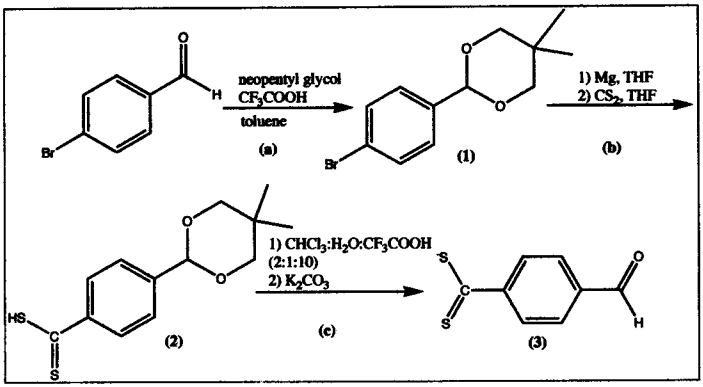

Figure 15. Synthesis of dithiolate linker to be added to quantum dot surface. (a) Protection of aldehyde with a glycol. (b) Exchange of bromine for dithiolate group via Grignard reaction. (c) Deprotection of aldehyde with acid.

Chemicals. All solvents and reagents were acquired from Aldrich unless otherwise noted.

Characterization Techniques. All precursors and synthesized ligands were identified by ^{1}H NMR spectroscopy on a Varian Gemini200 200-MHz NMR (solvent is noted for each individual sample). Samples containing quantum dots were characterized with a Hewlett-Packard 8452A Diode Array UV/Visible spectrophotometer (wavelength range 200 – 800 nm) and Photon Technology Quantamaster Fluorometer (excitation wavelength are noted for each data set).

3.1.1 Preparation of tailored quantum dots.

i) Preparation of Potassium 4-Formyldithiobenzoate.

a) 2-(4-bromophenyl)-5,5-dimethyl-1,3-dioxane (1). 4-Bromobenzaldehyde (3.7216 g, 20 mmol) and 2,2-dimethyl-1,3-propanediol (20.9220 g, 200 mmol) were dissolved in 120 mL of toluene in a round-bottomed flask under $N_{2(g)}$ and trifluoroacetic acid (0.461 mL, 6 x 10^{-3} mmol) was added. The mixture was heated to 90° C for 17 h. The reaction mixture was then washed with saturated potassium carbonate solution and then with water. The organic layer was concentrated and the product recrystallized in water to give 5.0 g (92% yield) of the white solid 2-(4-bromophenyl)-5,5-dimethyl-1,3-dioxane (1).

^{1}H NMR ($CDCl_3$, 200 MHz): δ 7.49 (dd, 2H), 7.39 (dd, 2H), 5.35 (s, IH), 3.61 (dd, 4H), 1.28 (s, 3H), 0.80 (s, 3H).

b) 4-(5,5-dimethyl-1,3-dioxan-2-yl)-dithiobenzoic acid (2). Dried Mg turnings (2.24 g, 92.18 mmol) were covered with 20 mL of anhydrous THF in a round-bottomed flask under nitrogen gas. Five grams (18.44 mmol) of (1) was dissolved in 40 mL of anhydrous THF and added dropwise to the Mg turnings. The mixture was stirred

vigorously under reflux for 2.5 h becoming brown in color. The solution was then transferred via cannula to a flask containing 3.34 mL (55.32 mmol) carbon disulfide in 50 mL anhydrous THF previously cooled to -5° - 0° C. The mixture was allowed to warm to room temperature while stirring overnight. The product was then hydrolyzed with 200 mL of 1:1 diethyl ether: water mixture. The aqueous layer was acidified with 200 mL 0.2M HCl and extracted with diethyl ether. The combined organic layers were washed two times with water, dried over magnesium sulfate, and concentrated to form a dark purple-red oil. The product was then crystallized in methanol to give 0.1563g (3.2%) of 4-(5,5-dimethyl-1,3-dioxan-2-yl)-dithiobenzoic acid (2).

^{1}H NMR ($CDCl_3$, 200 MHz): δ 7.939 (dd, 2H), 7.39 (dd, 2H), 6.20 (S-H, s, 1H), 5.40 (s, 1H), 3.68 (dd, 4H), 1.255 (dd, 3H), 0.810 (dd, 3H).

c) Potassium 4-formyldithiobenzoate (3). Water (0.5 mL) and concentrated TFA (5 mL) were added to a solution of (2) (100.8 mg, 0.373 mmol) in 1 mL of chloroform. The solution was stirred at room temperature for 4 h. The reaction mixture was diluted with 5 mL chloroform and neutralized with saturated potassium carbonate solution to form 4-formyldithiobenzoic acid in its potassium salt form (3) (11.5 mg, 14%).

^{1}H NMR (acetone d_6, 200 MHz): δ 10.08 (s, 1H), 8.14 (d, 2H), 7.99 (d, 2H).

The characterization of the above compounds was consistent with the literature.

ii) Preparation of aniline tetramer[27,28].

The free-base of N-phenyl-1,4-phenylenediamine (0.9627 g, 5.2 mmol) was dissolved in 100 mL of 1.0 M HCl with vigorous stirring and heating. The solution was cooled to 0° C in an ice water bath. Ferric chloride hexahydrate (2.924 g, 10.4 mmol) was dissolved

in 15 mL of 0.1M HCl at room temperature. This yellow solution was then cooled to 0° C and quickly added to the solution of dianiline hydrochloride. The blue mixture became pasty and was stirred mechanically for 4 h. The product was washed in a Buchner funnel 20x with 50 mL portions of 0.1M HCl and dried overnight. The product was then redispersed in deionized water for 2 h and subsequently deprotonated with 400 mL of 0.1M ammonium hydroxide (48 h). The product was separated by filtration and washed 14x with 40 mL portions of 0.1M ammonium hydroxide. The product was dried in a vacuum dessicator to give 0.4023g (21%) of aniline tetramer (4).

^{1}H NMR (anhydrous DMSO, 200 MHz): δ 8.37 (N-H, s, 1H), 7.25 (d, 2H), 7.04 (d, 4H), 7.0-6.7 (m, 9H), 6.67 (d, 2H), 5.56 (N-H_2, s, 2H).

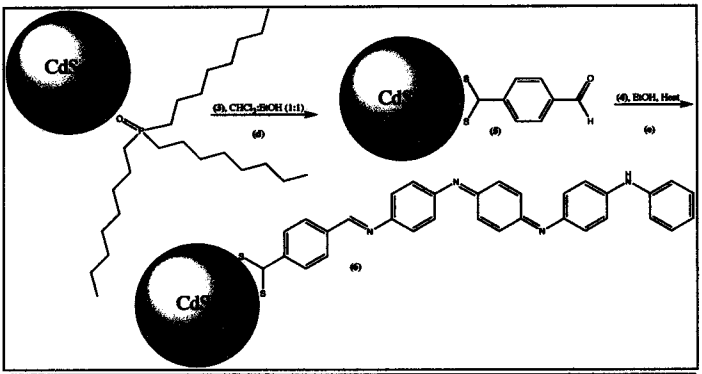

Figure 16. Functionalization of quantum dot surface with disulfide linker and aniline tetramer ligand. (d) Exchange of TOPO ligands for dithiolate linker. (e) Grafting of aniline tetramer.

iii) Grafting of disulfide linker and aniline tetramer onto nanocrystals.

d) Ligand exchange on surface of nanocrystal.

Trioctylphosphine oxide ligands are exchanged for potassium 4-formyldithiobenzoate ligand forming a disulfide bridge between the nanocrystal and the ligand.

Ligand (3) (3.7 mg, 0.0167 mmol) was placed under $N_{2(g)}$ in a round bottom flask and dissolved in 5 mL of ethanol. One milliliter (0.815 nmol) of Fort Orange CdSe/ZnS Quantum Dots (Evident Technologies) (60.31 μg/mL, Concentration: 8.15 x10^{-7} M, MW of core= 74 μg/nmol) in chloroform was added and allowed to stir at room temperature for 2 hr. The reaction mixture was purified by precipitation and washing with methanol. The product (5) was then redissolved in ethanol.

UV-Vis (ethanol): Broad band absorption, λ= 584 nm. Fluorescence Spectroscopy (ethanol), exc. at 360 nm: λ_{max}= 480 nm.

e) Grafting of aniline tetramer tether.

The solution of (5) was diluted with 4 mL ethanol in an inert atmosphere. Aniline tetramer (4) (10.2 mg, 0.0280 mmol) was dissolved in 3 mL of ethanol. The tetramer solution was added dropwise to the functionalized quantum dots and allowed to reflux overnight. The black precipitate was filtered and washed twice with methanol and then twice with chloroform. The product (6) (4.2 mg, Concentration = 1.56 x10^{-6} M, MW= 1.25x 10^{-7} mg/mmol) was allowed to dry and redissolved in 5 mL ethanol (0.84 mg/mL). (Note: The calculation of molecular weight of the final complex assuming that 100% ligand exchange took place on each quantum dot and no free quantum dots or free ligands remained in solution).

UV-Vis (0.084mg/mL in ethanol): λ_{max}= 311 nm, λ= 590 nm. Fluorescence Spectroscopy (0.084mg/mL in ethanol), exc. at 360 nm: λ_{max} 460 nm.

3.2 Results and Discussion

The functionalized quantum dot surfaces have many unique characteristics. The overlap of the ligands electronic energy levels with the quantum dot can allow charge transfer. In addition, the dithiolate linkage is more stable than the phosphines of the TOPO ligands.[29] Also, adequate surface passivation by the linker should prevent oxidation of the nanocrystal.

Figure 17 compares the emission of the linker and the emission of the linker after attachment to the quantum dot surface. Attachment is evident because a red shift in the

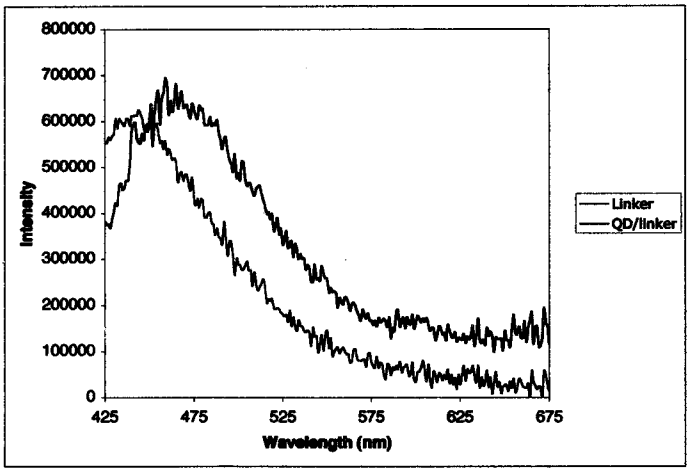

Figure 17. Red shift in linker peak indicates attachment. Excitation wavelength 360 nm.

emission due to the linker is observed. Further, Figure 18 confirms this because the quantum dot emission of the QD/Linker is completely quenched. This means that there cannot be quantum dot simply in solution with the linker; attachment must have occurred or the emission of the quantum dot would still be observed.

In addition, Figure 18 emphasizes the complete quenching of the QD/Linker/tetramer system. Absorption data shows that the quantum dot is still absorbing a broad range of light. While this specific functionalized quantum dot may not be useful in our proposed chemical sensor system, it could be useful in photovoltaic cells such as solar cells (Section 1.3). In the case of a solar cell, photons of light from the sun

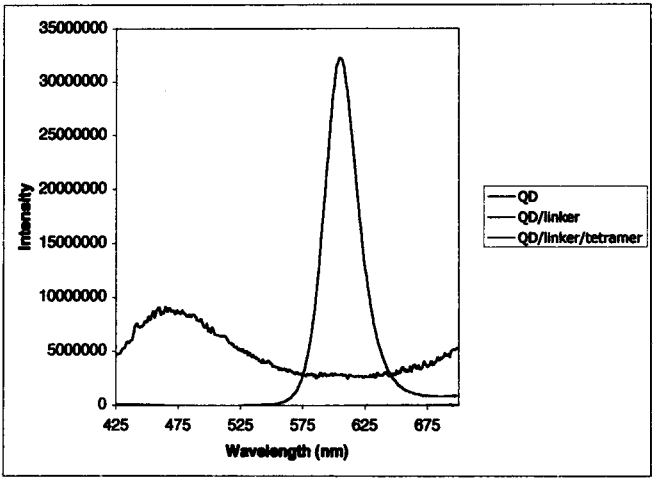

Figure 18. Emission QD, QD/linker, and QD/linker/tetramer. Excitation wavelength 360 nm.

would be absorbed by the quantum dot and be transferred from light energy to electrical current. Electrons could be transferred along the aniline conjugated pi system in the form of electrical energy.

4. Conclusions and Future Work

There are always ways to develop and redevelop research projects with different aims and focuses. The same is true for this research. There are many possible routes for the future of this research.

It would be advantageous to repeat the quantum dot concentration studies (Section 2) at higher loadings of quantum dot. Our research found that the 8.33 nmol QD loading was the best, but it was also the highest loading we prepared. It may be that higher concentrations of QD are needed to have a fully functional sensor system.

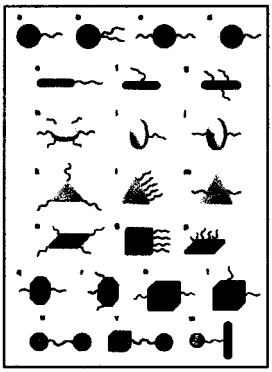

Figure 19. Possible quantum dot tether shapes. Adapted from Zhang, Z.L.; Horsch, M.A.; Lamm, M.H.; and Glotzer, S.C. *J. Am. Chem. Soc.* 2003. *3*. 1241.

Also, the preparation of a library of various QD/linker/tether systems (Section 3) should be synthesized and tested for emission quenching or enhancement (Figure 19). Enhanced emission of the quantum dots would be advantageous for the proposed nanocomposite sensor and should be included into Laponite clay for further studies. This would allow for alteration of the quantum dot (select quantum dot emission to match excitation of fluorescent Rhodamine monomer and J-aggregates), the linker[30] (amine[31], phosphines[32], oxygen, or other dithiolate linkages), and the tether (polyaniline[33], PPV[13], proteins[34], or DNA[35]).

In addition to fluorescence and UV/visible spectroscopy, these systems could be studied with X-ray diffraction (information about structural microenvironments of the

Laponite with the functionalized quantum dot), voltammetry[36] (electronic conductivity), or fluorescence lifetimes (changes in lifetimes of quantum dots when functionalized and when embedded into Laponite).

Finally, it is important to explore the potential applications for the quantum dot systems developed in this research. The proposed chemical sensor of Rhodamine/customizedQD/Laponite could be exposed to the hydrocarbons we hope to detect. These studies would provide insight on how to go about altering the system to obtain the best chemical sensor. These modifications might include using Na-Laponite instead of zinc-exchanged Laponite or utilizing a different functionalized quantum dot. Also, our QD/Laponite systems could be developed into light-emitting diodes to give more efficient QLED systems. Additionally, the QD/linker/tether system developed could be integrated into photovoltaic and solar cells to study the conversion of light energy into electrical current.

5. References

1. Whitesides, G. and Grzybowski, B. *Science,* **2002,** *295,* 2418-2421.

2. Walt, D.R. *Acc. Chem. Res.* **1998**, *31*, 267.

3. Colorado, R.; Villazana, R.J.; Lee, T.R. *Langmuir* **1998**, *14*, 6337.

4. Thompson, R.B.; Rasmussen, K.O.; Lookman, T. *Nano Letters* **2004**, *4*(12), 2455.

5. Joo, J.; Na, H.B.; Yu, T.; Yu, J.H.; Kim, Y.W.; Wu, F.; Zhang, J.Z.; Hyeon, T. *J. Am. Chem. Soc.* **2003**, *125*, 11100.

6. Carpenter, Michael. Presentation at Union College. Winter 2005.

7. Archermann, M.; Petruska, M.A.; Kos, S.; Smith, D.L.; Koleske, D.D.; and Kilmov, V. *Nature,* **2004**, *429*, 10.

8. Querner, C.; Reiss, P.; Bleuse, J.; and Pron, A. *J. Amer. Chem. Soc.* **2004**, *126*, 11574-11582.

9. Alvisatos, A.P. Perspectives on the Physical Chemistry of Semiconductor Nanocrystals. *J. Phys Chem.* **1996**, *100*, 13226.

10. www.evidenttech.com

11. Zhang, Jin. Presentation at National ACS meeting. San Diego, CA. March 2005.

12. Hoshino, A.; Fujioka, K.; Oku, T.; Suga, M.; Sasaki, Y.F.; Ohta, T.; Yasuhara, M.; Suzuki, K.; and Yamamoto, K. *NanoLetters* **2004**, *4*, 11, 2163-2169.

13. Puzder, A.; Williamson, A.J.; Zaitseva, N.; and Galli, G. *NanoLetters* **2004**, *4*, 12, 2361-2365.

14. Skaff, H.; Sill, K.; and Emrick, T. *J. Am. Chem. Soc.* **2004**, *126*, 11322-11325.

15. Osterloh, F.E.; Martino, J.S.; Hiramatsu, H.; and Hewitt, D.P. *NanoLetters.* **2003**, *3*. 125-129.

16. Wang, D.; Rogach, A.L.; and Caruso, F. *Nano Letters.* **2002**, *2*, 857-861.

17. Kieffel, Y., Travers, J.P.; Ermolieff, A.; and Rouchon, D. *Journal of Applied Polymer Science* **2002**, *86*, 395-404.

18. Mokari, T.; Sertchook, H.; Aharoni, A.; Ebenstein, Y.; Avnir, D.; and Banin, U. *Chem. Mater.* **2005** *17*(2), 258-263.

19. Martinez, V.M.; Arbeloa, F.L.; Prieto, J.B.; Lopez, T.A.; and Arbeloa, I.L. *Langmuir* **2004**, *20*(14), 5709-5717.

20. Hagerman, M.E.; Salamone, S.J.; Herbst, R.W., and Payeur, A.L. *Chem. Mater.* **2003**, *15*, 443-450.

21. Clapp, A.R.; Mendintz, I.L.; Fisher, B.R.; Anderson, G.P.; and Mattoussi, H. *J. Am. Chem. Soc.* **2005**, *127*, 1242-1250.

22. Clapp, A.R.; Mendintz, I.L.; Mauro, M., Fisher, B.R.; Bawendi, M.G.; and Mattoussi, H. *J. Am. Chem. Soc.* **2004**, *26*, 301-310.

23. Wargnier, R.; Baranov, A.V.; Maslov, V.G.; Stsiapura, V.; Artemyev, M.; Pluot, M.; Sukhanova, A.; and Nabiev, I. *NanoLetters* **2004**, *4*, 3, 451-457.

24. Zhao, J.; Zhang, J.; Jiang, C.; Bohnenberger, J.; Basche, T.; and Mews, A. *Journal of Applied Physics* **2004**, *96(6)*, 3206.

25. Brabec, C.J.; Sariciftci, N.S.; Hummelen, J.C. *Adv. Func. Mater.* **2001**, *11*(1), 15.

26. Arrandale, Mayrita. Union College Steinmetz Symposium, Spring 2005.

27. Dufour, B.; Rannou, P.; Travers, J.P.; and Pron, A. *Macromolecules* **2002**, *35*, 6112-6120.

28. Feng, J.; Zhang, W.; MacDiarmid, A.G.; and Epstein, A.J. *Annu. Technol. Conf. (ANTEC97)* **1997**, *2*, 1373-1377.

29. Love, J.C.; Estroff, L.A.; Kriebel, J.K.; Nuzzo, R.G.; and Whitesides, G.M. *Chem, Rev.* 105(*4*), 1103, 2005.

30. Potapova, I., Mruk, R., Prehl, S.; Zentel, R.; Basche, T.; and Mews, A. *J. Am. Chem. Soc.* **2003**, *125*, 320-321.

31. Talapin, D.V.; Rogach, A.L.; Kornowski, A.; Haase, M.; and Weller, H. *NanoLetters* **2001**, *1(4)*, 207.

32. Kim, S. and Bawendi, M.G. *J. Am. Chem. Soc. (Comm)* **2003**, *125*, 14652.

33. Porter, T.L.; Eastman, M.P.; Zhang, D.Y.; Hagerman, M.E. *J. Phys. Chem. B* **1997**, *101*, 11106-11111.

34. Chan, W.C.W.; and Nie, S. *Science* **1998**, *281*, 2016.

35. Mitchell, G.P.; Mirkin, C.A., and Letsinger, R.L. *J. Am. Chem. Soc.* **1999**, *121*, 8122-8123.

36. Greene, I.A.; Wu, F.; Zhang, J.Z.; and Chen, S. *J. Phys. Chem. B* **2003**, *107*, 5733-5739.